Numerical simulations of an Extreme AO system for an ELT

Richard Clare[1,a], Miska Le Louarn[1]

[1]European Southern Observatory, Adaptive Optics Systems Department, Karl Schwarzschild strasse 2, 85748 Garching bei Muenchen, Germany

Abstract. In this article, simulation results are presented for an extreme adaptive optics (order 200x200 sub-apertures) system, using a Pyramid WFS. These end-to-end simulations show that such a system is tractable with current simulation software and hardware. We also demonstrate that a novel reconstruction algorithm – CuRe – can provide similar performance (at much lower computational cost) than our standard Matrix Vector Multiply.

1. Introduction

The purpose of this paper is to attempt the computationally challenging task of numerically simulating an extreme adaptive optics (XAO) for an extremely large telescope (ELT). To achieve this, we use the ESO end-to-end AO simulation tool Octopus [1]. We simulate a high order XAO system, aimed at obtaining high contrast images to be used for extra-solar planet detection. This is done using a modulated pyramid wavefront sensor-based system, on a 42m telescope. Also, we compare the AO performance of two reconstruction algorithms – the traditional matrix-vector-multiply (MVM) with the recently introduced Cumulative Reconstructor CuRe [2][3].

In Section 2, we present the XAO system and simulation parameters. The simulation results for these parameters are shown in Section 3. In Section 4, the conclusions are drawn.

2. Simulation and XAO System Parameters

In this Section, we define the simulation and system parameters for the XAO system.

The XAO system we are modelling is for a 42m diameter telescope, with central obstruction, but without spiders or segmentation. The evaluation metric is Long Exposure (LE) Strehl in K band (2.2µm) on-axis only. Each simulation is run over 500 iterations, which takes of the order of 3-7 hours on the AO simulation cluster (depending on the modulation width). The XAO system uses a visible pyramid wavefront sensor of order 200x200 pixels (subapertures). The most important parameters for the XAO system are shown in Table 1.

The controller for the XAO simulations in this paper is a simple integrator. The loop gain of the integrator is optimized for each flux level simulated.

---

[a] e-mail : lelouarn@eso.org

Table 1. XAO system parameters.

WFS subapertures	Frame Rate	WFS λ	read noise	DM order	Total slopes / actuators	Modulation Width	Delay
Pyramid 200x200	3 kHz	0.7 μm	2.8 e / pixel	201x201	57592 / 29618	4λ/D	2 frames

The default reconstructor U used in these simulations is a *maximum a posteriori* (MAP) MVM reconstructor [4],

$$U = (B^T C_N^{-1} B + C_\emptyset^{-1})^{-1} B^T C_N^{-1}, \tag{1}$$

where B is the push-pull interaction matrix and C_N and $C_\emptyset$ are the noise and atmospheric covariance matrices respectively.

The assumed atmosphere in this paper is a 9 layer median one derived from statistics at Paranal [5]. The Fried parameter r_0 for this profile is 12.9cm at 0.5μm (and the seeing 0.75'') and the outer scale L_0 is 25m. The 9 layer atmosphere is tabulated in Table 2.

Table 2. Atmospheric model used for the simulations.

Layer	Height (m)	% of C_N^2	Wind Speed (m/s)
1	47	53.28	15
2	140	1.45	13
3	281	3.5	14
4	562	9.57	10
5	1125	10.83	9
6	2250	4.37	15
7	4500	6.58	25
8	9000	3.71	40
9	18000	6.71	21

3. XAO Simulation Results

In this section, we present the simulation results for the parameters defined in Section 2. First of all, we optimize the modulation width of the pyramid sensor with respect to the flux level of the NGS. In Fig. 1, the LE Strehl in K band is plotted versus the detected NGS photon flux per subaperture per frame. We see that for higher flux levels, the modulation widths of 2λ/D, 4λ/D and 6λ/D yield similar performance of a Strehl of ~0.96. However, the Strehl is much more sensitive to the modulation width at lower flux – especially the 5 photons/subaperture/frame point. We choose a modulation width of 4λ/D for the remainder of the simulations in this paper. Note that the more modulation is introduced, the longer the simulation takes, since each modulation point is simulated by 8 individual pyramid positions. So a modulation of 6λ/D is actually 48 times more computationally intensive than without modulation. This was not really a problem for us, since our simulation tool is fully parallelized, and therefore adding modulation steps could be handled by adding CPUs working on the calculations.
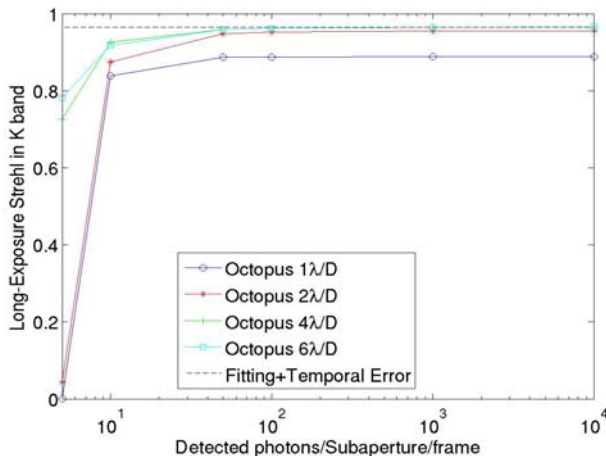
Fig. 1. Strehl in K band versus NGS photon flux for different modulation widths of the pyramid. The dashed line is the sum of the fitting and temporal errors.

In Fig. 1, we also check that the Strehl at high flux for the simulations matches that predicted by theory for the fitting and temporal error terms. The fitting and temporal errors are given respectively by [6]

$$\sigma_{fitting}^2 = 0.26(d/r_0)^{(5/3)}, \tag{1}$$
$$\sigma_{delay}^2 = 6.88(VT/r_0)^{(5/3)}, \tag{2}$$

where d is the subaperture spacing, r_0 is the Fried parameter, V is the characteristic wind speed, and T is the delay. The LE Strehl in K band after 500 iterations with 1e4 photons/subaperture/frame and 2.8e read noise/pixel for the median profile is 0.967. This is with the loop gain optimized to 0.7. By using Equations (1) and (2), for the fitting and

temporal errors for the median atmospheric profile, the theoretical Strehl in K band for this XAO system is 0.965, showing good agreement with the high flux simulation.

Fig. 2 shows the K band Strehl versus modulation width for the highest flux point of Fig. 1 – 10^4 photons/subaperture/frame. The chosen modulation of $4\lambda/D$ is optimal at this flux level.
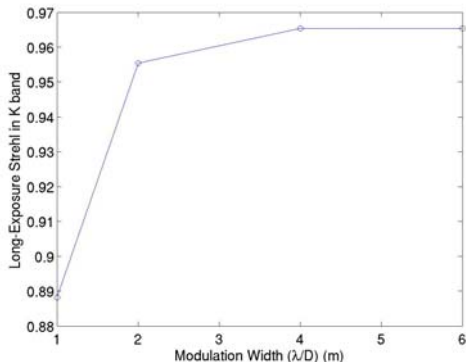
Fig. 2. Strehl in K band versus modulation widths of the pyramid for a detected photon flux level of 10^4 photons/subaperture/frame.

While we use Strehl in K band as the default metric in this paper, it is insightful for XAO systems to also investigate the structure of the point spread function (PSF). In Fig. 3, the PSFs in K band are plotted for modulation widths of $2\lambda/D$ and $6\lambda/D$ for the high flux case. For reference, the K band Strehl is 0.965 for $2\lambda/D$ and 0.955 for $6\lambda/D$. The PSFs exhibit the typical high-Strehl shape of a "dark hole" corrected by the AO system, which is easily visible, thanks to the small sensitivity of the pyramid sensor to aliasing. While the K band Strehls for the two cases are almost identical, there is a noticeable difference between the two PSFs.
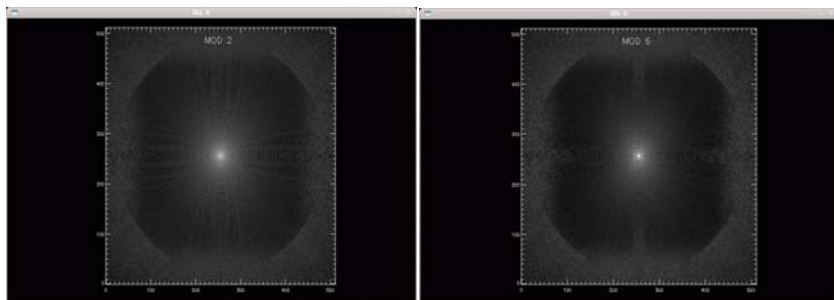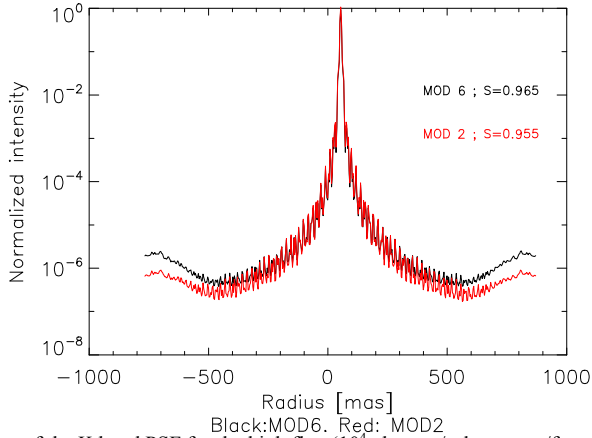

Fig. 3. The K band PSF for high flux (10^4 photons/subaperture/frame) for modulation widths of $2\lambda/D$ (left) and $6\lambda/D$ (right). The pixel scale is 5.3 mas/pixel.

The difference between the two PSFS can be seen by plotting the radial average of the two PSFs in Fig. 4. The wings of the PSF for the modulation $2\lambda/D$ case are lower than those of the

6λ/D case, and thus give a better contrast at the larger angle. Depending on the science case (i.e. in which region the planets are sought), this difference may be significant for the system's capability to find exo-planets.

Fig. 4. Radial average of the K band PSF for the high flux (10^4 photons/subaperture/frame) for modulation widths of 2λ/D (red) and 6λ/D (black).

Another result of interest for XAO is the shape of the PSF for different imaging wavelengths. So far we have investigated K band (2.2μm) only. In Fig. 5, we plot radial averages of the PSF for J (1.25 μm), H (1.65μm) and K bands. We can see that although the Strehl ratio is significantly reduced (in K-band, 0.96, 0.89 in the J-band), a non-negligible improvement of the PSF is still obtained in the J-band.
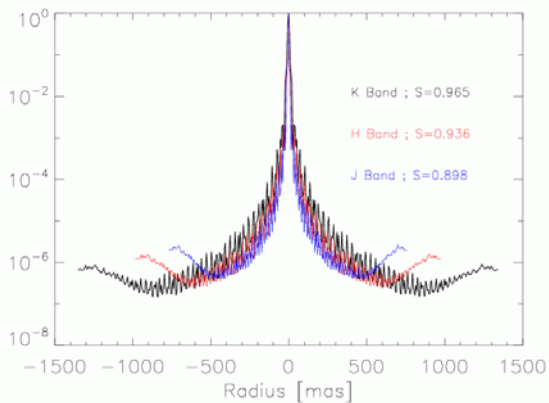

Fig. 5. Radial average of the PSF for J (blue), H (red) and K (black) bands for the high flux case (10^4 photons/subaperture/frame) and with modulation of 4λ/D.

We are also interested in the speed of loop convergence for different flux levels. In Fig. 6, the K band short exposure (SE) Strehl is plotted versus the first 100 iterations for both the 5 and 50 photons/subaperture/frame cases. For the 50 photon case, the ultimate Strehl of ~0.95 is attained by 60 iterations, while for the 5 photon case, the SE is improving marginally up to 100 iterations. We can conclude from this that even for a low degree of correction (at low flux), the pyramid sensor does not exhibit any particular difficulty at closing the loop. It could have been argued that since the Strehl ratio of the PSF at the tip of the pyramid (always at 0.7um), the sensor would have been in a more non-linear regime, hence making closing the loop more difficult. There is no sign of this, perhaps because the Strehl ratio is still good enough to form a diffraction limited core on the tip of the sensor, even at 0.7µm.

Finally, we investigate a new reconstructor developed for the Austrian in-kind contribution for ESO. This new reconstructor is CuRe. We compare the performance of CuRe in terms of Strehl and PSF shape to that of the MVM reconstructor used previously in this paper. CuRe is a computationally efficient reconstruction algorithm (of order N), which performs wavefront reconstructions significantly faster (less operations, which are well pipelineable) than with the MVM.
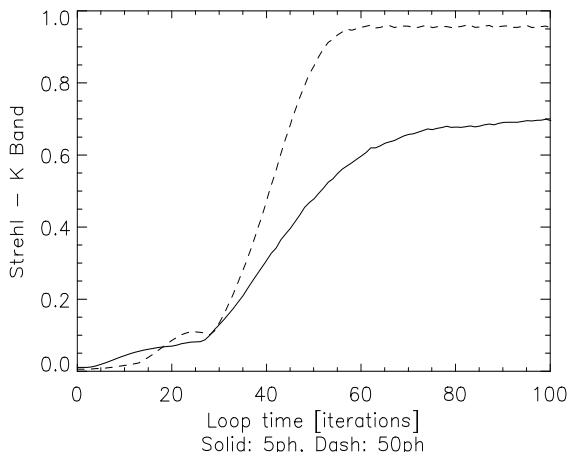

Fig. 6. Short Exposure Strehl in K band versus iteration number for 5 photons/subaperture/frame (solid line) and 50 photons/subaperture/frame (dashed line).

Several variations of the algorithm have been developed, in order to improve its performance. The most basic version (a simple cumulative reconstruction) was the initial attempt to use such a reconstructor. The result, which is shown on the left of Fig. 7, is not very good at reconstructing the highest spatial frequencies, which shows as an increased halo towards the outer edge of the PSF. Once this problem was identified, the algorithm was improved by several methods, with steps of pre-processing of the slopes and post processing of the calculated command, and a domain decomposition approach in the reconstruction itself to

reduce noise propagation. These steps significantly improve the performance of the algorithm, as demonstrated on the figure on the left – where the halo is significantly lowered. This can be seen in more detail in Fig. 8, which shows radially averaged cuts of the PSFs. We can see that the improved algorithm comes very close to the original MVM method, but with much less operations than the conventional MVM, which will allow the real time computer for such a system to be greatly simplified. These curves also show how a reconstruction algorithm can be improved to perform better, thanks to the comparison with an already existing "reference" algorithm. These improvements greatly boosted the CuRe's performance, and were done without sacrificing the computational speed advantage of the method.
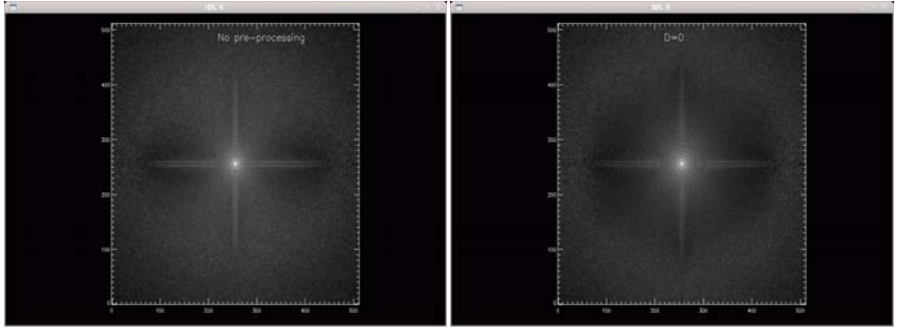
Fig. 7. K band PSFs for the CuRe reconstructor for the high flux case without pre- and post-processing and domain decomposition (left), and CuRe with those refinements (right).
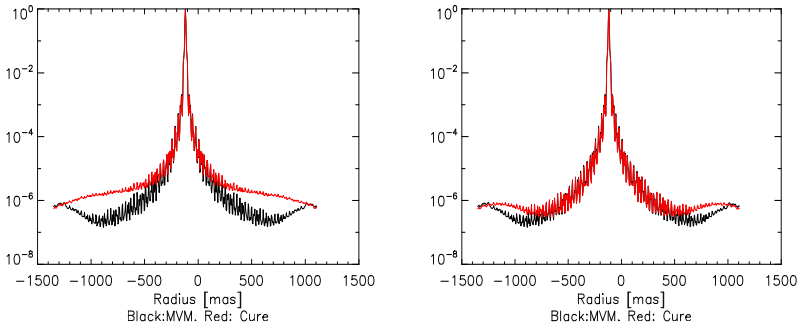
Fig. 8. The red curves are the radial average of the K band PSFs for the high flux case for CuRe without pre- and post-processing and domain decomposition (left), and CuRe with those refinements (right). The black curves are the radial average of the K band PSF for the high flux case for the MVM.

4. Conclusions

In this paper, we have demonstrated that end-to-end simulations of an extreme AO system (of order 200x200 "sub-apertures") using a modulated pyramid sensor are feasible today with our software and hardware. We have also shown that similar AO performance can be obtained with the novel CuRe reconstruction algorithm as the standard MVM, but with the advantage of much lower computational load (in the reconstruction process) for the novel method.

5. References

1. M. le Louarn, C. Verinaud, V. Korkiakoski, and E. Fedrigo, "Parallel simulation tools for AO on ELTS," in *Advancements in Adaptive Optics*, Proc. SPIE 5490 (2004).
2. M. Rosensteiner, JOSA A, **28**, 10, pp. 2132, (2011)
3. M. Zhariy, A. Neubauer, M. Rosensteiner, R. Ramlau, Cumulative Wavefront Reconstructor for the Shack-Hartman Sensor, in Inverse Problems and Imaging, 2012, accepted.
4. N. F. Law et al., "Wavefront estimation at low light levels," Opt. Commun. **126**, 19-24 (1996).
5. G. Lombardi et al., "Combining turbulence profiles from MASS and SLODAR: a study of the evolution of the seeing at Paranal," Proc. SPIE 7012, 701221 (2008).
6. C. Bechet et al., "Performances of the fractal iterative method with an internal model control law on the ESO end-to-end ELT adaptive optics simulator," in *Adaptive Optics Systems,* Proc. SPIE 7015 (2008).